Journal of Power Sources 196 (2011) 968–976

Contents lists available at ScienceDirect

Journal of Power Sources

journal homepage: www.elsevier.com/locate/jpowsour

Anode- versus electrolyte-supported Ni-YSZ/YSZ/Pt SOFCs: Effect of cell design on OCV, performance and carbon formation for the direct utilization of dry methane

Marco A. Buccheri, Anand Singh, Josephine M. Hill*

Department of Chemical and Petroleum Engineering, University of Calgary, 2500 University Dr. NW, Calgary, Alberta, T2N 1N4, Canada

ARTICLE INFO

Article history:
Received 22 June 2010
Received in revised form 26 August 2010
Accepted 26 August 2010

Keywords:
Solid oxide fuel cell
Ni/YSZ anode
Carbon deposition
Direct methane utilization
Anode-supported cell
Electrolyte-supported cell

ABSTRACT

In this study, anode- and electrolyte-supported Ni-YSZ/YSZ/Pt solid oxide fuel cells (SOFC) are compared in terms of performance and carbon formation when operated on dry methane. Although anode-supported SOFCs are typically used in industry, electrolyte-supported cells may be required for certain laboratory experiments. Thermodynamic calculations were performed to calculate the equilibrium gas-phase composition. The measured open circuit voltages (OCV) in dry methane were 1.15 V and 0.92 V for anode- and electrolyte-supported cells, respectively. The difference in these OCV values reflects the different gas-phase compositions at the electrochemically active region of the two cell designs. The conduction layer in the anode-supported SOFC provides the catalytic sites to produce more hydrogen, which results in a higher OCV and a larger limiting current density. Over time, carbon is also produced and results in a higher degradation rate on the anode-supported cell. Carbon also forms on the electrolyte-supported cell but has less of a negative impact on the operation of the electrolyte-supported cell. Temperature-programmed oxidation (TPO) studies indicate that the carbon formed in the conduction layer of an anode-supported cell is much more stable and difficult to remove than carbon formed on the functional layer.

1. Introduction

Solid oxide fuel cells (SOFCs) are fuel flexible and have an operating temperature in the range of 773–1273 K that favors reforming reactions and fast kinetics [1]. Nickel (Ni) is the conventional catalyst material for the anode of an SOFC and is an excellent steam reforming catalyst. Hence, in practice, it is possible to reform hydrocarbons internally in the anode compartment of SOFC, but a steam to carbon ratio (S/C) greater than two is generally required to avoid carbon deposition [2]. The disadvantages of internal reforming are lower open circuit voltage (OCV), lower electrical efficiency, and temperature gradients in the anode structure originating from the different extents of reaction as a function of location – endothermic steam reforming at the outer region, and exothermic electrochemical oxidation in the inner region [2,3].

Direct utilization, in which the feed contains only the hydrocarbon without steam or other oxidant, increases the efficiency of the system, and reduces thermal gradients due to a reduction in steam reforming, but may result in faster degradation of the anode due to carbon deposition [2,4–6]. With methane as a fuel, carbon may deposit on the metal surface and then dissolve into the bulk of the metal at temperatures above 873 K [7]. With feeds other than methane, carbonaceous compounds can also be formed by free-radical, gas-phase-condensation reactions (pyrolytic carbon) further blocking pores and increasing mass transfer resistance to and from the triple phase boundary (TPB) [6]. The morphology and reactivity of the carbon formed at the anode of a SOFC vary [8] and depend on fuel and anode material selection, steam to carbon ratio, operating conditions, etc. [7–9].

The direct utilization of the following fuels has been investigated: methane [4,10–17], propane [11,12,15], butane [4,11,13,18], diesel [5], methanol [19], and ethanol [20] in both anode- and electrolyte-supported cells. Various anode compositions have been used for these studies including noble and non-noble metals, fluorites, and perovskites. Ceria-based anodes, with a fluorite structure, have a high resistance to carbon deposition. For example, McIntosh et al. [18] impregnated a porous YSZ matrix with 10 wt% CeO_2 and 20 wt% Cu, and exposed these anodes to *n*-butane, *n*-decane, toluene and propane for various periods of time. Only minor amounts of carbonaceous deposits formed and these deposits actually increased the electronic conductivity in the Cu/YSZ anode resulting in higher performance rather than deactivation of the cell. The addition of Ni, Co and/or noble metals, such as Pt, Rh, Pd and

* Corresponding author. Tel.: +1 403 210 9488; fax: +1 403 284 4852.
E-mail address: jhill@ucalgary.ca (J.M. Hill).

0378-7753/$ – see front matter © 2010 Elsevier B.V. All rights reserved.
doi:10.1016/j.jpowsour.2010.08.073

Ru, to ceria are beneficial in terms of the reforming reactions of hydrocarbons [17,21].

Other potential materials for the direct utilization of hydrocarbons with a perovskite structure are doped-$LaCrO_3$ and doped-$SrTiO_3$ [21]. Liu et al. [12] tested a composite anode made of $La_{0.8}Sr_{0.2}Cr_{0.8}Mn_{0.2}O_{3-\delta}$ (LSCM) and an ionic conductive ceramic $Ce_{0.9}Gd_{0.1}O_{1.95}$ (GDC) with 4 wt% Ni. The cell was exposed to propane and butane and little or no coking was observed. Without Ni, the cell had negligible performance and a low open circuit voltage (OCV) of ~0.65 V. Thus, Ni enhanced the electrochemical performance and reforming activity of the anode.

Ni has several advantages, including low cost, ease of fabrication, high electrochemical activity, high reforming activity, and high electronic conductivity, in comparison to other potential anode materials for SOFC. The main disadvantages of Ni are susceptibility to carbon deposition and mechanical instability under redox cycling. A Ni/yttria-stabilized zirconia (YSZ) anode-supported cell has been operated directly on methane for 160 h at 973 K without coking [10]. The stable performance was a result of the lower operating temperature and high operating current density ($\geq$800 mA cm^{-2}). No characterization of the carbon deposition on the anode structure at the end of the 160 h test was reported.

Previous work in our group [7–9,22] has demonstrated how carbon deposition on a Ni/YSZ anode is affected by the operating current density, duration of exposure, feed conditions, temperature and the anode thickness. Specifically, increasing the current density and using an anode in which all of the Ni was part of the TPB (<25 μm thick functional layer) resulted in significantly less carbon deposition. The carbon that did form on the functional layer was easier to remove than that formed on the conduction layer suggesting that the water formed in situ and/or the presence of O^{2-} ions influenced the carbon deposition. Because of these factors, it may be difficult to compare different cell designs. Although a large fraction [23] of the SOFC made by companies are anode-supported, in the laboratory there are reasons for preparing both anode- and electrolyte-supported cells. For example, three-electrode work, in which the processes at each electrode can be analyzed independently, is easier on electrolyte-supported cells.

Thus, in this study, the role of the cell design on carbon formation and electrochemical performance was investigated so that results obtained on different cell designs can be appropriately compared. Specifically, anode- and electrolyte-supported cells with Ni/YSZ based anodes have been tested for their performance at 1023 K with a dry methane feed. A thermodynamic analysis has been performed to predict the gas-phase composition within the anode compartment and whether carbon is thermodynamically favored at the operating conditions. The cells were tested for electrochemical stability under a constant load and characterized using electrochemical impedance spectroscopy (EIS), as well as scanning electron microscopy (SEM). Temperature-programmed oxidation (TPO) was used to determine the type of carbon formed during the stability tests. The results confirm that the cell design, specifically the thickness of the conduction layer, significantly influences the performance of the cells and the nature of the carbon formed.

2. Thermodynamic calculations and experimental methods

2.1. Thermodynamic calculations

Thermodynamic analysis was done numerically using the software CEA (Chemical Equilibrium with Applications) developed by NASA as previously reported [24]. This method determines the chemical equilibrium composition by the minimization of the Gibbs free energy of the gas in the anode compartment (Eq. (1)).

$$(dG_{sys})_{p,T} = 0 \quad (1)$$

and employs Lagrange's method of the undetermined multipliers to determine a solution [25].

The procedure involves writing an expression for the total Gibbs energy of the system and then finding the composition which minimizes G_{sys} for a given temperature and pressure, subject to the constraints of the material balances [25]. The Gibbs free energy of formation of the chemical species is used for the calculations and does not require the assumption of any chemical reactions [26]. The ideal gas law is the equation of state used in the calculations for the low pressure and high temperatures typical for SOFC anode conditions.

2.2. Anode- and electrolyte-supported cell preparation and testing

Electrolyte-supported cells were prepared by uni-axial pressing YSZ powder (Tosoh, TZ-8Y) into disks 25 mm in diameter. The electrolyte disks were sintered in air at 1723 K for 4 h. The electrolyte was dense, free of pinholes and approximately 500 μm thick. A NiO/YSZ slurry was prepared by ball milling NiO (Alfa Aesar, 99%) and YSZ powder, in the mass ratio of 1:1, with zirconia milling media in ethanol for 24 h. The mixture was dried and ground in a mortar followed by sieving to obtain particles less than 150 μm in size. A liquid carrier, α-terpineol (Alfa Aesar), was added to the sieved powders and the resulting slurry was painted onto the electrolyte. The electrolyte and anode slurry were dried at 350 K and sintered at 1623 K for 4 h in air with heating and cooling rates of 5 K min^{-1}. After sintering, the anode thickness was approximately 50 μm with a geometric area of 0.3 cm^2. The cathode was applied by painting Pt paste (Engelhard) onto the electrolyte and firing the assembly at 1173 K in air for 1 h. Ag wires were attached to the electrodes as current collectors. Pt paste was used to attach the wire to the cathode side and Ag paste was used to connect the wire to the NiO/YSZ anode. The cell was placed at the end of an alumina cell holder with a 14 mm inner diameter. Glass paste (ESL 4460, The Hydrogen Co.) was used to seal the anode side of the cell onto the cell holder, while the cathode side was left exposed to air.

Anode-supported cells were prepared by uni-axial pressing the electrolyte and anode material simultaneously. The anode material was a mixture of NiO (50 wt%), YSZ (43 wt%) and graphite (7 wt%). Graphite (Alfa Aesar, conductive grade, 325 Mesh) was added to the NiO/YSZ mixture to enhance porosity in the thick electrode. The electrolyte and anode were co-sintered at 1623 K for 4 h with heating and cooling rates of 1 K min^{-1}. The different shrinkage rates of the electrolyte (YSZ), and the NiO/YSZ anode caused deformation and cracks of the cell. This problem was overcome by placing a mass of ~250 g on the electrolyte/anode disks during sintering. Similar to the electrolyte-supported design, the cathode was made by painting Pt paste on the electrolyte and had a geometric area of 0.3 cm^2.A ceramic-based sealing paste (Aremco, 552 VFG) was used to seal the anode-supported cell onto the cell holder. Ag wires were attached to the anode and cathode by Ag and Pt paste, respectively.

For electrochemical testing, the cells were heated to the operating temperature in He and the anodes were then reduced in H_2 at 1023 K for 1 h. Electrochemical measurements were performed using a standard electrochemical interface (1287 Potentiostat + 1260 FRA, Solartron Analytical). The flow rate was maintained constant throughout the experiments and equal to 50 ml min^{-1} (STP) for humidified hydrogen and 25 ml min^{-1} (STP) for dry methane. Electrochemical impedance spectroscopy (EIS) experiments were performed at 1023 K and open circuit voltage (OCV) for cells exposed to humidified hydrogen (flow rate of 50 ml min^{-1}) and dry methane (flow rate 25 ml min^{-1}). The flow rate for methane was half of the flow rate of hydrogen to maintain a constant total molar flow rate of hydrogen. Impedance spectroscopy analysis was performed at OCV with a perturbation of

10 mV amplitude in the frequency range 10^5–0.1 Hz. Stability tests were performed at a constant current density of 50 mA cm^{-2} and 100 mA cm^{-2}, for electrolyte- and anode-supported cells, respectively, in dry methane (flow rate of 25 ml min^{-1}) at 1023 K.

2.3. Characterization of cells

Temperature-programmed oxidation (TPO) was used to characterize and quantify any carbon formed after the stability tests. The cells were cooled in He after the galvanostatic tests and then transferred to an alumina tube for the TPO analysis. TPO was done with 10% O_2 in He with a flow rate of 50 ml min^{-1} (STP). The temperature was increased from room temperature to 1173 K at 10 K min^{-1} and the outlet gases were analyzed with a mass spectrometer (Cirrus, MKS Spectra products). Signals for m/z = 44 (CO_2), m/z = 28 (CO), m/z = 32 (O_2), m/z = 18 (H_2O) and m/z = 2 (H_2) were monitored during the TPO experiment. The signals for CO_2 and H_2O were calibrated with gas mixtures of known concentrations. Scanning electron microscopy (SEM) (Philips XL30 ESEM) was used to investigate the morphology of the carbon deposits and anodes after testing in dry methane. The samples were broken after the stability tests and sputtered with gold to reduce charging in the SEM.

Three cells of each type (anode- or electrolyte-supported) were prepared for the stability experiments. After exposure to dry methane for 24 h, two of the cells were cooled in He and then used for the TPO and SEM analysis. The third cell was exposed to humidified H_2 for 1 h at OCV to investigate whether the original cell performance could be restored.

3. Results and discussion

3.1. Equilibrium composition

Fig. 1 shows the thermodynamic equilibrium composition of the carbon and gas species as a function of temperature in the anode compartment of an SOFC operated with dry methane. The methane is essentially completely decomposed by 1100 K. Solid carbon (C_s) and hydrogen are thermodynamically favoured for temperatures above 600 K. The predicted composition is consistent with the cracking of methane (Eq. (2)) being the sole reaction. Our results are consistent with another study [27] in which a different software package (HSC Chemistry) was used.

$$CH_4 \rightarrow C_s + 2H_{2_g} \quad \Delta H_r^\circ = 75\,\text{kJ mol}^{-1} \tag{2}$$

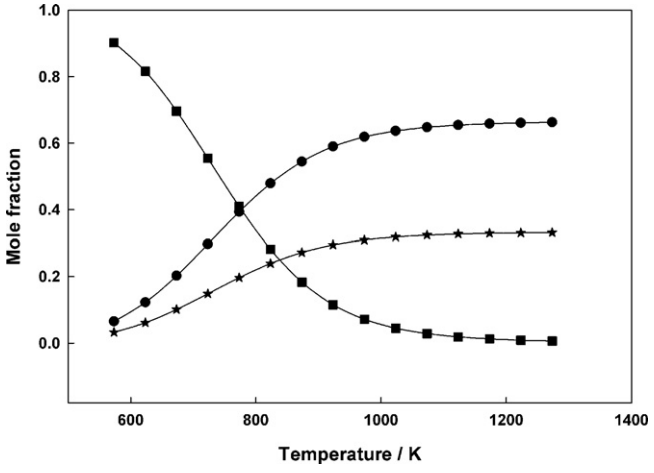

Fig. 1. Equilibrium composition as a function of temperature for a dry methane feed at 1 atm. The species at equilibrium are CH_4 (■), H_2 (●) and C_s, graphite (⋆).

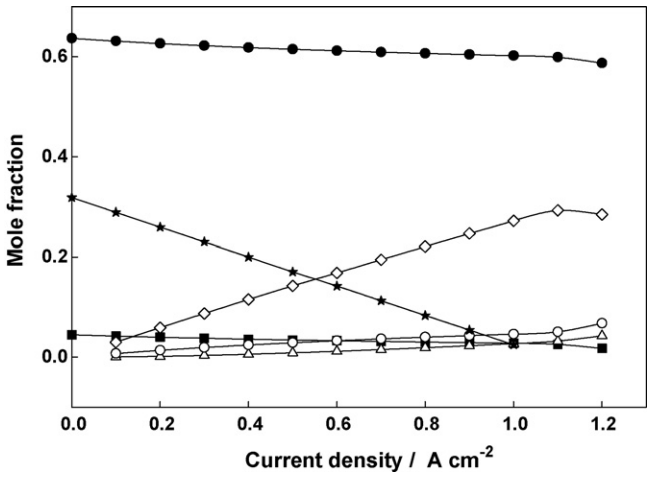

Fig. 2. Equilibrium composition as a function of current density for dry methane feed (25 ml min^{-1}) at 1023 K and 1 atm. The species at equilibrium are CH_4 (■), CO (◊), CO_2 (△), H_2 (●), H_2O (○) and C_s, graphite (⋆).

For an SOFC in operation (i.e., under a constant load), a flux of oxygen ions is supplied to the anode compartment and must be considered in the calculations. The input of oxygen to the anode compartment at a given current density can be calculated by Faraday's law (Eq. (3)).

$$n_{O_2} = \frac{i}{zF} \tag{3}$$

where n_{O_2} is the flow of oxygen (mol s^{-1} cm^{-2}) delivered to the anode, i is the current density (A cm^{-2}), F is Faraday's constant (96487 C mol^{-1} equivalent) and z = 4 is the number of electrons involved in the oxygen reduction reaction (Eq. (4)).

$$O_2 + 4e^- \rightarrow 2O^{2-} \tag{4}$$

Fig. 2 shows the equilibrium composition of the carbon and gas species as a function of current density for a SOFC operated at 1023 K and 1 atm with dry methane feed (25 ml min^{-1}). The presence of oxygen anions produces the species CO, CO_2, and H_2O in addition to H_2 and C_s. The mole fraction of CH_4 decreases from ~0.04 to essentially 0 as the current density increases from 0.1 A cm^{-2} to 1 A cm^{-2}.

At low operating current density (<0.4 A cm^{-2}), the predominant chemical species are C_s and H_2. As the current density increases, the amount of solid carbon present decreases, possibly by the electrochemical oxidation of carbon (Eq. (5)) and/or the reaction of water (Eq. (6)) with carbon.

$$C_s + O^{2-} \rightarrow CO + 2e^- \tag{5}$$

$$C_s + H_2O \rightarrow CO + H_2 \qquad \Delta H_r^\circ = 131\,\text{kJ mol}^{-1} \tag{6}$$

At intermediate current densities (0.4–1 A cm^{-2}), H_2 is still the main component but the concentration of CO continues to increase. CO is produced by the endothermic steam reforming reaction (Eq. (7)) and/or the partial oxidation of methane (Eq. (8)).

$$CH_4 + H_2O \rightarrow CO + 3H_2 \qquad \Delta H_r^\circ = 206\,\text{kJ mol}^{-1} \tag{7}$$

$$CH_4 + O^{2-} \rightarrow CO + 2H_2 + 2e^- \tag{8}$$

The production of CO may also be a result of the oxidation of carbon deposits (Eq. (5)) as suggested in other studies [2,26], and/or the reaction of water with carbon (Eq. (6)). At intermediate current densities, the equilibrium concentrations of CO_2 and H_2O are negligible.

At high operating current densities (>1 A cm^{-2}), solid carbon is not thermodynamically predicted and the CO_2 and H_2O concentrations increase. CO_2 may be produced by the direct electrochemical

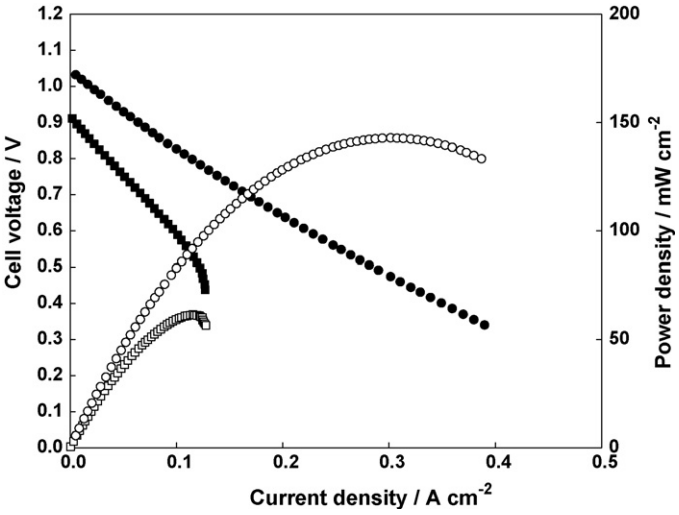

Fig. 3. Power density (open symbols) and cell voltage (filled symbols) as a function of current density for humidified H_2 (○, ●) and dry CH_4 (□, ■) with flow rates of 50 and 25 ml min^{-1} respectively for a Ni/YSZ electrolyte-supported SOFC at 1023 K.

oxidation of methane (Eq. (9)) as suggested by Koh et al. [26], and/or the exothermic water gas shift reaction (Eq. (10)). H_2O is a product of the electrochemical oxidation of hydrogen (Eq. (11)) and/or methane (Eq. (9)).

$$CH_4 + 4O^{2-} \rightarrow CO_2 + 2H_2O + 8e^- \quad (9)$$

$$CO + H_2O \rightarrow CO_2 + H_2 \qquad \Delta H_r^\circ = -41\ \text{kJ mol}^{-1} \quad (10)$$

$$H_2 + \frac{1}{2}O_2^{2-} \rightarrow H_2O + 2e^- \quad (11)$$

3.2. Electrochemical measurements

Electrolyte- and anode-supported cells were tested with dry methane at 1023 K to investigate how the cell design affects the electrochemical/reforming reactions and the deposition of carbon. The current-voltage characteristics and power density curves of electrolyte- and anode-supported cells are shown in Figs. 3 and 4, respectively. For the electrolyte-supported cell, an OCV value of 1.08 V was measured in humidified H_2, which is close to the calculated value of 1.09 V and indicated that the cell was well-sealed. The OCV in dry methane was 0.92 V, which is lower than the theoretical value of 1.15 V calculated for the direct oxidation of methane (Eq. (9)). Maximum power densities of 140 mW cm^{-2} and 60 mW cm^{-2} were obtained in humidified H_2 and dry CH_4, respectively. A limiting current density of approximately 120 mA cm^{-2} was obtained in CH_4.

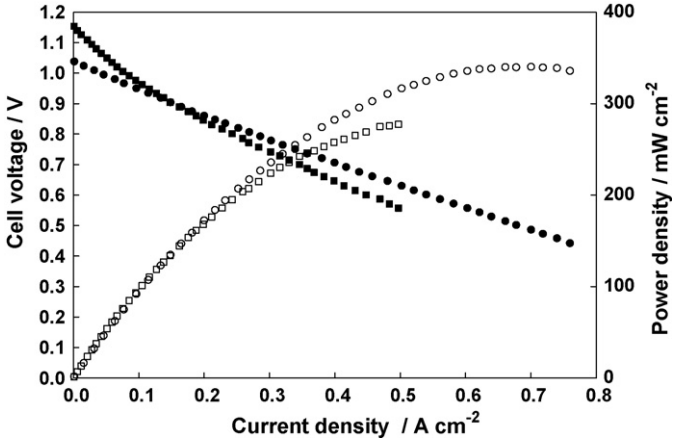

Fig. 4. Power density (open symbols) and cell voltage (filled symbols) as a function of current density for humidified H_2 (○, ●) and dry CH_4 (□, ■) with flow rates of 50 ml min^{-1} and 25 ml min^{-1} respectively for a Ni/YSZ anode-supported SOFC at 1023 K.

Because the Ni/YSZ anode was ~50 μm thick, the limiting current density cannot be explained by mass transfer limitations to the triple phase boundary (TPB), but rather as a limited supply of the reactants that are oxidized at the anode. The catalyst amount may be insufficient to convert CH_4 into H_2 by the cracking reaction (Eq. (2)) at the same rate that hydrogen is being consumed by the electrochemical reaction (Eq. (11)) at higher current densities resulting in a limiting current density. This situation is consistent with an OCV (0.92 V), which is less than the calculated value for CH_4, and may be associated with a reduced H_2 partial pressure at the anode TPB. The low OCV in dry methane for an electrolyte-supported configuration was not attributed to failure of the sealing as the OCV was restored to the value of 1.08 V when the fuel was switched to humidified hydrogen. Eguchi et al. [28] have also reported measured OCV values lower than theoretical for an electrolyte-supported cell operated with methane reformed internally on a Ni/YSZ anode. The lower OCV was explained by the insufficient amount of catalyst to completely reform the fuel. Gorte et al. [4] reported an OCV of 0.9 V for CH_4 at 973 K with a Cu–CeO_2 anode-supported cell, and this low OCV was interpreted by the equilibrium established between the hydrocarbons and the partial oxidation products.

For the anode-supported cells, the OCV values were 1.05 V and 1.15 V in humidified H_2 and dry CH_4, respectively, and the limiting current density was greater than 0.5 A cm^{-2} (Fig. 4). The maximum power densities were 320 mW cm^{-2} in humidified H_2 and 280 mW cm^{-2} in dry CH_4. These values are approximately two and five times higher than the values for the electrolyte-supported cells. A higher OCV for an anode-supported configuration has been reported in other studies with similar cells [10]. In the anode-supported cell configuration, the YSZ electrolyte is thinner (~200 μm) resulting in a lower ohmic resistance and, thus, higher power density. This result suggests that an anode-supported cell mostly affects the utilization of methane such that the power density curve for dry CH_4 is closer to that for H_2. A thicker anode enhances the cracking activity and increases the hydrogen partial pressure at the TPB resulting in a higher OCV and an increase in the limiting current density.

Fig. 5 shows the impedance spectra at OCV for an electrolyte-supported cell before and after the stability test in dry CH_4. Before the stability test, the high frequency intercept with the real axis (R_Ω) was fuel (humidified H_2 or dry CH_4) independent at 1.2 Ω cm^2. This value exceeds the calculated ohmic resistance of 1.1 Ω cm^2 for a 500 μm-thick YSZ with a ionic resistivity of 22.3 Ω cm at1073 K [29]. The impedance spectra are in the form of depressed arcs that were larger for dry CH_4 than humidified H_2. Polarization resistances (R_p) of approximately 1 Ω cm^2 and 1.8 Ω cm^2 were measured at OCV for humidified H_2 and dry CH_4, respectively. The R_p is given by the difference between the low frequency intercept (R_T) and the ohmic resistance (R_Ω).

After the stability test, the high frequency intercept (R_Ω) for the impedance measured in dry CH_4 increased to 2.5 Ω cm^2. This change in ohmic resistance is likely because of the degradation of contact between anode and current collector during the experiment as typically the ohmic resistance is relatively stable. The R_p also increased substantially to 11.5 Ω cm^2. An increase in R_p may result from carbon blocking the pores and increasing diffusion resistance and/or carbon deposition on the Ni particles, which may decrease the TPB available for the electrochemical oxidation of the fuel. After the stability test, the cell was exposed to humidified H_2 for 1 h at OCV (flow rate of 50 ml min^{-1} and 1023 K), and

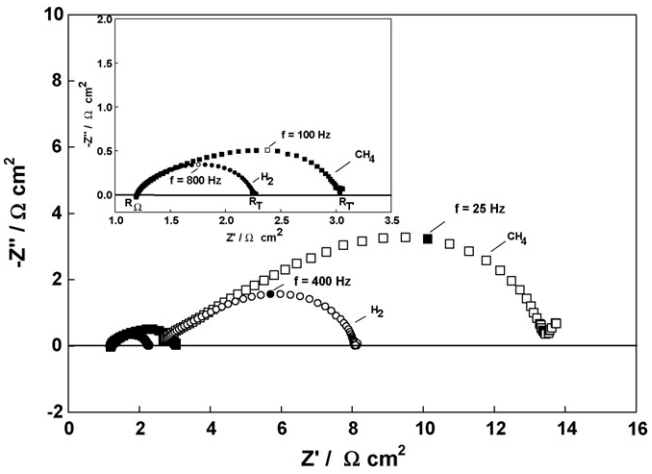

Fig. 5. Equilibrium impedance for an electrolyte-supported cell in humidified H_2 (●,○) and dry CH_4 (■,□) before (filled symbols) and after (open symbols) stability test (16 h, 1023 K, dry CH_4 feed, 50 mA cm^{-2}). Inset is an expansion of the impedance real axis. The cell was exposed to humidified H_2 for 1 h at OCV after the stability test before the impedance was measured. Markers correspond to the frequencies labeled.

the impedance measured again to see if the original performance could be recovered in this time. The polarization resistance was 5.5 Ω cm^2 and the performance was not restored completely during this period. This degradation may be due to several factors including irreversible damage of the anode structure by carbon deposition, sintering of Ni with consequent reduction of TPB, and/or mobility of the Ag paste to reduce the connection between the current collector and the anode. The ohmic resistance did not change when the fuel was switched back to hydrogen after the stability test, which is consistent with a decrease in connectivity between the current collector and the anode over the course of the experiment.

Fig. 6 shows the impedance spectra at OCV for an anode-supported cell before and after the stability test. Before the stability test, the impedance spectrum consisted of a depressed arc that was larger for dry methane than for humidified hydrogen as for the electrolyte-supported cells (insets of Figs. 5 and 6). The high frequency intercept was 0.46 Ω cm^2 and was similar for both fuels. The polarization resistance was approximately 0.64 Ω cm^2 in humidified hydrogen and 1.06 Ω cm^2 in dry methane, both values being approximately half of the values measured for the electrolyte-

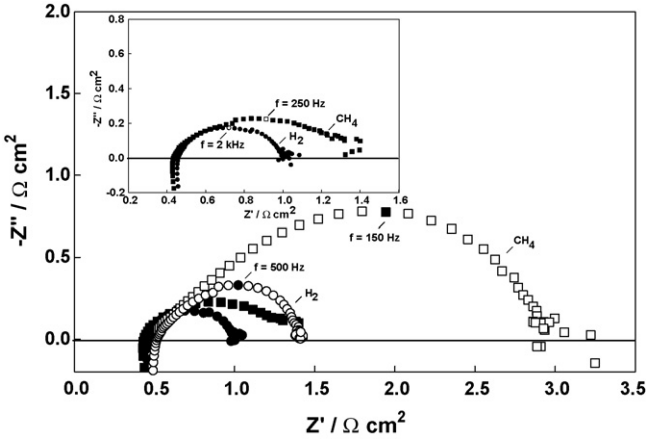

Fig. 6. Equilibrium impedance for an anode-supported cell in humidified H_2 (●,○) and CH_4 (■,□) before (filled symbols) and after (open symbols) stability test (24 h, 1023 K, dry CH_4 feed, 100 mA cm^{-2}). Inset is an expansion of the impedance real axis. The cell was exposed to humidified H_2 for 1 h at OCV after the stability test before the impedance was measured. Markers correspond to the frequencies labeled.

supported cells. After the stability test, the R_Ω value increased only slightly, while the R_p value increased significantly to approximately 2.49 Ω cm^2. The increase in polarization resistance, as was also observed for electrolyte-supported cells, may be a result of carbon damaging the anode and blocking pores. Exposing the anode to hydrogen for 1 h at OCV reduced the R_p to 0.98 Ω cm^2 but the original R_p was not recovered.

In the case of a single reaction on a uniform electrode, the faradaic impedance (Z_f) can be represented as a charge transfer resistance (R_{ct}). The representation is, however, more complicated for the interfacial response if coupled reactions, reactions involving mass transfer, reactions involving adsorbed species, and reaction on non uniform surfaces are involved [30]. Another factor that adds complexity to the impedance interpretation analysis in full cell studies is the presence of the cathode and its contribution to the spectrum. The entire cell voltage was measured to be consistent with both cell types – it is difficult to position a reference electrode on anode-supported cells. Nevertheless, the cathode was identical in the two cells types and thus, changes in the impedance spectra can be attributed to changes in the anode. Because EIS was performed at OCV with an amplitude of 10 mV, mass transport limitations can also be neglected and the faradaic impedance (or total R_p) being a charge transfer resistance is a good approximation. Thus, the differences in R_p between different cell tests and cell types can now be entirely attributed to changes in R_{ct} at the anode. The measured resistances for the six cells used in this study are shown in Table 1.

The cells of each type were relatively consistent in their measured resistance values for each condition before the stability tests. The one exception is Cell 3 of the electrolyte-supported cells that had a significantly higher R_p value after exposure to methane. Likely the current collector came loose during the experiment. In humidified hydrogen, the average R_p values for anode- and electrolyte-supported cells were 0.84 Ω cm^2 and 1.9 Ω cm^2, respectively, indicating that the anode-supported cells may have faster electron transfer kinetics. The anodes in the two cell types were prepared by different techniques, which will affect the microstructure and performance of the cells. The anode-supported cells were prepared by pressing and co-sintering the anode and electrolyte; while the anode in the electrolyte-supported cell was brush painted onto the electrolyte.

3.3. Cell stability and carbon deposition

Electrolyte- and anode-supported cells were tested at constant current densities of 50 mA cm^{-2} and 100 mA cm^{-2}, respectively, with dry CH_4. Carbon deposition is thermodynamically favoured at these current densities (Fig. 2) and so the effects of carbon deposition and subsequent degradation of the cell voltage can be investigated. The electrolyte-supported cell was operated at 50 mA cm^{-2} while the anode-supported cell was operated at twice that current density because a better cell performance in dry methane was achieved for this cell at similar total cell voltage. Fig. 7 shows the results of the galvanostatic (stability) experiments for the two cell types. These results are representative of the results for the six cells that were tested (three of each type). The voltage of the electrolyte-supported cell decreased by 150 mV in the first 3 h and then was essentially constant for the rest of experiment. In contrast, the performance of the anode-supported cell was not stable and the voltage fluctuated with an average degradation rate (slope of the regression line for the data) of 8 mV h^{-1}. Koh et al. [31] reported similar behaviour for a Ni/YSZ anode-supported cell operating in dry CH_4 and attributed the degradation to carbon deposition by visual inspection. The trends seen in the stability tests herein are consistent with carbon formation.

Table 1
Impedance data for the tested cells.

Sample	Before stability test						After stability test					
	H_2 (3% H_2O)			CH_4			CH_4			H_2 (3% H_2O)		
	R_Ω (Ω cm^2)	R_P (Ω cm^2)	R_T (Ω cm^2)	R_Ω (Ω cm^2)	R_P (Ω cm^2)	R_T (Ω cm^2)	R_Ω (Ω cm^2)	R_P (Ω cm^2)	R_T (Ω cm^2)	R_Ω (Ω cm^2)	R_P (Ω cm^2)	R_T (Ω cm^2)
Anode-supported cells												
Cell 1 (EIS analysis)	0.46	0.64	1.1	0.44	1.06	1.5	0.51	2.49	3	0.52	0.98	1.5
Cell 2 (TPO analysis)	0.69	1.5	2.2	0.63	2.67	3.3	Cooled in He			Cooled in He		
Cell 3 (SEM analysis)	0.63	0.37	1	0.64	1.96	2.6	Cooled in He			Cooled in He		
Electrolyte-supported cells												
Cell 1 (EIS analysis)	1.2	1	2.2	1.2	1.8	3	2.5	11.5	14	2.5	5.5	8
Cell 2 (TPO analysis)	1.1	1.1	2.2	1.2	5.9	7.1	Cooled in He			Cooled in He		
Cell 3 (SEM analysis)	1.2	3.6	4.8	3	262	265	Cooled in He			Cooled in He		

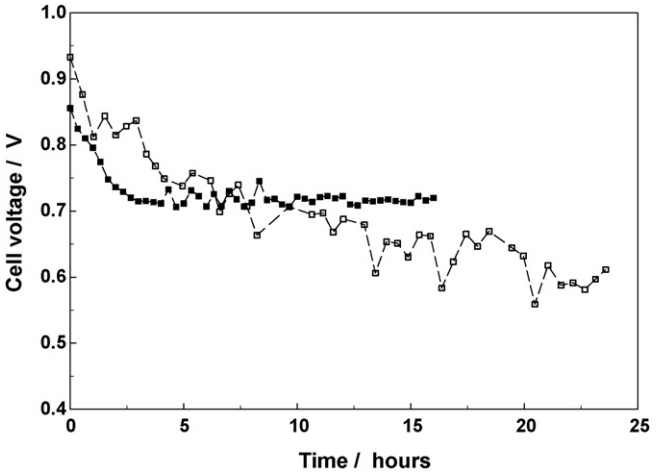

Fig. 7. Galvanostatic tests in dry CH_4 at 1023 K for an electrolyte-supported cell at a constant current density of 50 mA cm^{-2} (■), and for an anode-supported cell at a constant current density of 100 mA cm^{-2} (□).

Following the exposure to dry methane for 16 h or 24 h, TPO experiments were performed on the two cell types to characterize any carbon formed. Fig. 8a compares the CO_2 production during the TPO analysis of the Ni/YSZ anodes tested in the stability test (Fig. 7). Note that both the CO_2 and H_2O responses for the anode-supported cell have been multiplied in order that the tem-

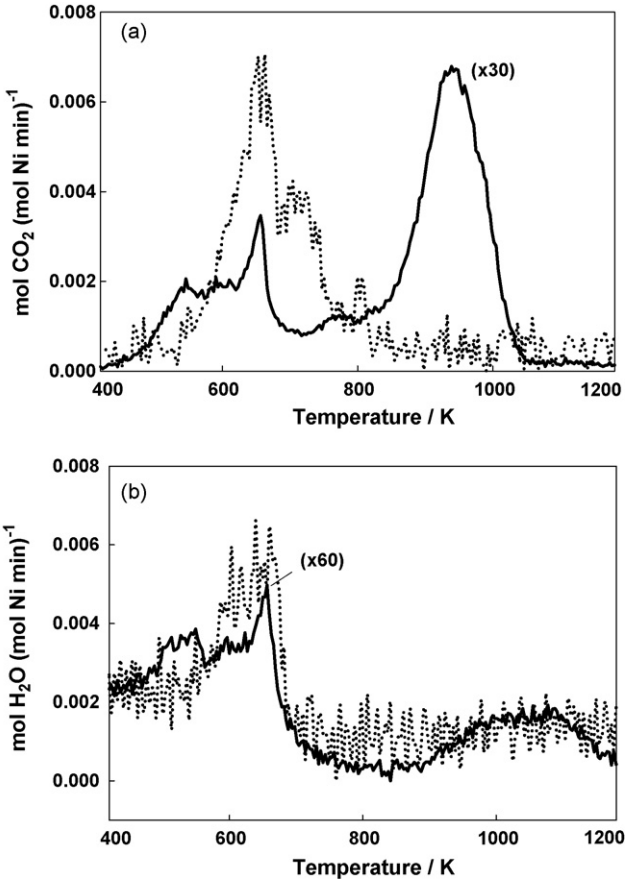

Fig. 8. CO_2 (a) and H_2O (b) production during TPO for an electrolyte-supported cell (dotted line) with a Ni/YSZ anode exposed to dry methane and constant current density of 50 mA cm^{-2} for 16 h; and for an anode-supported cell (solid line) exposed to dry methane and constant current density of 100 mA cm^{-2} for 24 h.

peratures for the peaks for the two cell types can be more easily compared. For the electrolyte-supported cell (dotted line), CO_2 was observed between 500 K and 800 K, as has been seen previously [8] for cells exposed to CH_4 at similar current densities. For the anode-supported cell (solid line), peaks were evident in two temperature regions. The first region corresponds to temperatures between 500 K and 700 K. The second region corresponds to higher temperatures between 800 K and 1050 K, and represents a more stable carbon similar to the carbon deposited on a Ni/YSZ anode operated at open circuit potential [8]. Water was also monitored during the TPO experiment and Fig. 8b shows the water signals for the two cell types.

The higher temperature peak in the TPO spectra is likely related to graphite formation. The XRD analysis of Ni/YSZ pellets exposed to humidified methane (see Fig. 2 in [7]) contained a peak at ~27° 2-theta that corresponds to graphite. Peaks for Ni carbide species (Ni_3C at ~45° 2-theta) were not present; Ni carbide is not expected as it forms at lower temperatures. In other work [32], the carbon deposited on a Ni/YSZ anode exposed to a feed of methane at 988 K was observed to be graphitic by in situ Raman spectroscopy analysis.

In absolute terms, significantly more carbon was formed on the anode-supported cell but normalization of the amounts of carbon with the amount of Ni in the anodes resulted in the following values: 0.005 mol C mol^{-1} Ni for the anode-supported cell compared to 0.160 mol C mol^{-1} Ni for the electrolyte-supported cell. These values may have significant standard errors because of the difficulty in accurately measuring the Ni content of the anodes. In addition, the Ni/YSZ anode from the anode-supported cell turned to powder after the stability test (metal dusting, see photo in [7]), making it difficult to collect all of the sample. The anode-supported cells are also more difficult to seal and any leaks will allow oxygen to react with the deposited carbon. Oxygen leaks would be consistent with the fluctuating voltage seen in Fig. 7. Given the results of the stability test, the type of carbon deposited is just as important, if not more so, than the amount of carbon. The H:C ratio in the deposited carbon was 0.50 and 1.13 for the anode- and electrolyte-supported cells, respectively.

SEM images of Ni/YSZ anodes after reduction in hydrogen for the anode-and electrolyte-supported cells are shown in Fig. 9a and b, respectively. Note that the magnifications of these images are different given the different size of anodes (800 μm for the anode-supported cell and approximately 50 μm for the electrolyte-supported cell). Fig. 9c and d show the Ni/YSZ anodes of the anode- and electrolyte-supported cells, respectively. The microstructure of the reduced anode in the anode-supported cell (Fig. 9c) appears to be less sintered than the reduced anode in the electrolyte-supported cell (Fig. 9d). The triple phase boundary (TPB) cannot be determined directly from the SEM images but a larger TPB length is expected for anode-supported cells given the lower values of R_p for this type of cell.

Images of the anodes after the stability test are given in Fig. 9e–g. The breakdown of the anode structure within the conduction layer of the anode-supported cell is visible in Fig. 9g. Carbon has destroyed the Ni particles as seen in ex-situ tests in which Ni/YSZ was exposed to humidified methane at 1073 K [7]. In contrast, the anode in the functional layer of the anode-supported cell has generally retained its structure, and the deposited carbon is granular or sponge-like (Fig. 9e). A similar type of carbon formed on the anode of the electrolyte-supported cell after the stability test (Fig. 9f). This type of carbon was observed by Alzate-Restrepo and Hill [8] for a Ni/YSZ anode exposed to humidified methane for 6 h at 1073 K with current densities of 10 mA cm^{-2} and 1 mA cm^{-2}. Note that the anodes examined in the SEM after the stability tests were not exposed to hydrogen as was done for the impedance measurements.

3.4. Discussion

The objective of this work was to study the impact of cell design for Ni-YSZ/YSZ/Pt SOFCs operated on dry methane on cell performance. The anode in anode-supported cells can be considered to consist of two different regions: a functional layer and a conduction layer; with different roles. The electrochemical reactions (Eqs. (5), (8), (9) and (11)) occur at the triple phase boundary (TPB) in the functional layer and the thickness of this region depends on the structure and composition, but may extend between 10 μm and 120 μm [14,33] from the electrolyte. The conduction layer provides support to the cell, supplies the fuel to the TPB, and provides electronic conductivity. With fuels other than hydrogen, the conduction layer also may catalyze the reforming and/or decomposition of the fuels. The anode in the electrolyte-supported cells used in this study nominally had a thickness of only 50 μm and may be considered to act only as Ni/YSZ functional layer.

Our results indicate that the two cell designs provide different results both in terms of electrochemical performance (OCV, power density, and stability) and type of carbon deposited. These differences stem, in part, from the different gas-phase compositions within the anode chamber and at the TPB in the two cells types. The thermodynamic calculations (Figs. 1 and 2) provide a guideline for the system if it is allowed to reach equilibrium. For systems that are operated on dry feeds, the likelihood of carbon formation increases with temperature. In contrast, in systems operating with humidified feeds [27] or feeds containing oxygen (e.g., alcohols) [24,27], the propensity for carbon deposition decreases as the temperature increases. At a fixed temperature, carbon formation decreases with increasing current density (Fig. 2).

Differences in microstructure that arise from the different preparation methods required to prepare either anode- or electrolyte-supported cells also influenced performance. The polarization resistance was lower for the anode-supported cells in hydrogen and dry methane (Table 1). The SEM analysis showed that the microstructure for the two cell types was not identical (Fig. 9c and d). There are limited techniques that can produce anodes with consistent microstructures over a range of thicknesses: 20 μm (electrolyte-supported cells) to 1000 μm (anode-supported cells). Plasma spraying [34] and traditional tape casting are methods that have this capability.

A range of OCV values between 0.9 V and 1.4 V [4,13,35] has been observed in the literature for SOFC operation in dry or humidified methane at temperatures between 973 K and 1273 K. Liu and Barnett [36] report that the measured OCV for Ni/YSZ anodes in humidified methane is in agreement with that calculated with the partial oxidation of carbon deposits (Eq. (5)) (~1.13 V at 1023 K, interpolating from Fig. 5 in Ref. [36]). The authors also mentioned, however, that multiple anode reactions may occur simultaneously and influence the OCV value. In another study [16], the OCV was attributed to the total oxidation of methane (Eq. (9)), and for these studies the OCV was usually greater than 1.15 V. In this work we suggest that the measured OCV (Figs. 3 and 4) values are a result of mixed-potentials. The mixed-potential is a non-equilibrium condition at net zero current and to be calculated requires the application of thermodynamics, kinetics and transport phenomena [30]. With the direct utilization of methane in SOFCs, several electrochemical oxidation reactions (Eqs. (5), (8), (9) and (11)) are possible on the anode, and each of these electrochemical reactions have a different Nernst potential as well as different kinetics. Thus, calculation of the mixed-potential for our system is beyond the scope of this paper.

The mixed-potential at OCV is more likely to be influenced by the hydrogen Nernst potential (calculated by Eq. (11)) given that the direct electrochemical oxidation of CH_4 (Eq. (9)) has more sluggish kinetics [17] than the electrochemical oxidation of hydrogen

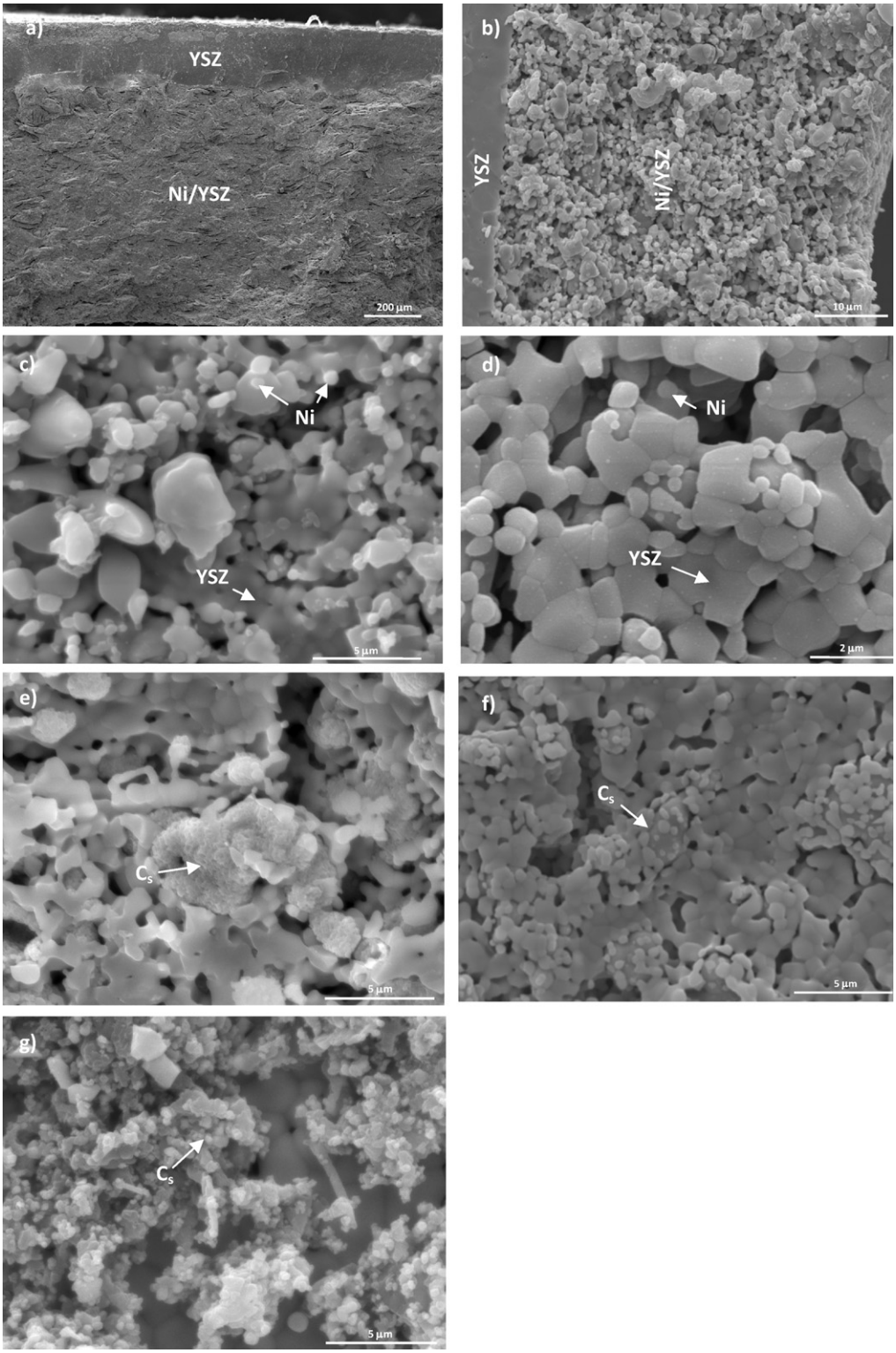

Fig. 9. SEM cross-sectional images of: (a) anode-supported cell, (b) electrolyte-supported cell; Ni-YSZ anodes in (c) anode-supported cell, (d) electrolyte-supported cell; functional layers in (e) anode-supported cell after stability test, (f) electrolyte-supported cell after stability test; and (g) conduction layer in anode-supported cell after stability test.

(Eq. (11)). In this study the OCV was lower for the electrolyte-supported cell (0.92 V, Fig. 3) than for the anode-supported cell (1.15 V, Fig. 4). The presence of a conduction/reforming layer in the anode-supported cell catalyzed the production of hydrogen and thus, increased the local partial pressure of hydrogen at the TPB. This suggestion is consistent with the work of Liu et al. [12], in which the addition of a reforming catalyst on a LSCM anode increased the OCV and enhanced performance by increasing the production of hydrogen within the anode. Similarly, the addition of C-H bond cracking catalysts to ceria (doped or un-doped) anode materials resulted in an increase of the OCV [15,37–39] because more H_2 was available. The lower limiting current density for the

electrolyte-supported cells also supports the theory that hydrogen and not methane is the species being oxidized at the anode under the conditions of this study.

Galvanostatic tests in dry methane (Fig. 7) showed that stability and behaviour of the electrolyte-and anode-supported cells was different. The performance of the electrolyte-supported cell was relatively stable after the first three hours of operation, while the performance of the anode-supported cell fluctuated and overall continued to degrade over the 24 h test. The results of the impedance (Figs. 5 and 6), TPO (Fig. 8) and SEM (Fig. 9) analysis are consistent with carbon deposition causing some, if not all, of the degradation. The carbon that has deposited is more reactive and contains a higher H:C ratio on the electrolyte-supported cell than on the anode-supported cell, and thus, even though there appears to be more carbon deposition on this cell, the degradation effect is less. In contrast, the carbon that forms on the anode-supported cell is less reactive (i.e., removed at a higher temperature in the TPO analysis) and resulted in more structural damage (Fig. 9g). The oscillating behaviour of the anode-supported cell (Fig. 7) may be a result of a cycle of carbon deposition and removal due to leaks in the anode compartment of the cell.

4. Conclusions

The equilibrium composition was calculated as a function of temperature and as a function of current density at one temperature (1023 K). Electrolyte-and anode-supported Ni-YSZ/YSZ/Pt cells were characterized and tested for their performance with dry methane feeds at 1023 K using operating conditions that were within the region in which solid carbon is expected at equilibrium. A higher initial OCV and power density were obtained on the anode-supported cells but these cells were less stable and suffered significant structural damage from carbon formation over a 24 h galvanostatic test. The difference in performance was attributed to the presence of a conduction layer in the anode-supported cells that catalyzed the formation of hydrogen such that the partial pressure of hydrogen at the TPB was higher than in the electrolyte-supported cell. This conduction layer also catalyzed carbon deposition that had a detrimental impact on the cells because the carbon destroyed the structure of the anode. For electrolyte-supported cells, the carbon deposition was not as severe. Differences in microstructure arose from the different preparation techniques (brush painting versus pressing and co-sintering) and also may have influenced the performance of the cells.

Acknowledgements

The present work was supported through funding to the NSERC Solid Oxide Fuel Cell Canada Strategic Research Network from the Natural Sciences and Engineering Research Council (NSERC) and other sponsors listed at www.sofccanada.com. The authors thank Dr. M. Cimenti for helpful discussions.

References

[1] A. Atkinson, S. Barnett, R.J. Gorte, J.T.S. Irvine, A.J. McEvoy, M. Mogensen, S.C. Singhal, J. Vohs, Nat. Mater. 3 (2004) 17–24.
[2] M. Mogensen, K. Kammer, Annu. Rev. Mater. Res. 33 (2003) 321–331.
[3] K. Nikooyeh, A.A. Jeje, J.M. Hill, J. Power Sources 171 (2007) 601–609.
[4] R.J. Gorte, S. Park, J.M. Vohs, C. Wang, Adv. Mater. 12 (2000) 1465–1469.
[5] R.J. Gorte, J.M. Vohs, J. Catal. 216 (2003) 477–486.
[6] S. McIntosh, R.J. Gorte, Chem. Rev. 104 (2004) 4845–4865.
[7] H. He, J.M. Hill, Appl. Catal., A 317 (2007) 284–292.
[8] V. Alzate-Restrepo, J.M. Hill, Appl. Catal. A342 (2008) 49–55.
[9] V. Alzate-Restrepo, J.M. Hill, J. Power Sources 195 (2009) 1344–1351.
[10] Y. Lin, Z. Zhan, J. Liu, S.A. Barnett, Solid State Ionics 176 (2005) 1827–1835.
[11] B.D. Madsen, S.A. Barnett, Solid State Ionics 176 (2005) 2545–2553.
[12] J. Liu, B.D. Madsen, Z. Ji, S.A. Barnett, Electrochem. Solid State Lett. 5 (2002) A122–A124.
[13] M.K. Bruce, M. van den Bossche, S. McIntosh, J. Electrochem. Soc. 155 (2008) B1202–B1209.
[14] A. Abudula, M. Ihara, H. Komiyama, K. Yamada, Solid State Ionics 86–88 (1996) 1203–1209.
[15] T. Hibino, A. Hashimoto, M. Yano, M. Suzuki, M. Sano, Electrochim. Acta 48 (2003) 2531–2537.
[16] M.D. Gross, J.M. Vohs, R.J. Gorte, Electrochem. Solid State Lett. 10 (2007) B65–B69.
[17] O.A. Marina, M. Mogensen, Appl. Catal. A 189 (1999) 117–126.
[18] S. McIntosh, J.M. Vohs, R.J. Gorte, J. Electrochem. Soc. 150 (2003) A470–A476.
[19] M. Cimenti, J.M. Hill, J. Power Sources 195 (2010) 54–61.
[20] M. Cimenti, J.M. Hill, J. Power Sources 195 (2010) 3996–4001.
[21] C. Sun, U. Stimming, J. Power Sources 171 (2007) 247–260.
[22] K. Nikooyeh, R. Clemmer, V. Alzate-Restrepo, J.M. Hill, Appl. Catal. A 347 (2008) 106–111.
[23] J. Larminie, A. Dicks, Fuel Cells Systems Explained, 2 ed., John Wiley & Sons Ltd, West Sussex, UK, 2003, pp. 207–226.
[24] M. Cimenti, J.M. Hill, J. Power Sources 186 (2009) 377–384.
[25] J.M. Smith, H.C.V. Ness, Introduction to Chemical Engineering Thermodynamics, 4 ed., McGraw-Hill, New York, 1987, pp. 532-542.
[26] J.-H. Koh, B.-S. Kang, H.C. Lim, Y.-S. Yoo, Electrochem. Solid State Lett. 4 (2001) A12–A15.
[27] K. Sasaki, Y. Teraoka, J. Electrochem. Soc. 150 (2003) A878–A884.
[28] K. Eguchi, H. Kojo, T. Takeguchi, R. Kikuchi, K. Sasaki, Solid State Ionics 152–153 (2002) 411–416.
[29] F. Zhao, A.V. Virkar, J. Power Sources 141 (2005) 79–95.
[30] M.E. Orazem, T. Bernard, Electrochemical Impedance Spectroscopy, John Wiley & Sons, Inc, 2008.
[31] J.-H. Koh, Y.-S. Yoo, J.-W. Park, H.C. Lim, Solid State Ionics 149 (2002) 157–166.
[32] M.B. Pomfret, J. Marda, G.S. Jackson, B.W. Eichhorn, A.M. Dean, R.A. Walker, J. Phys. Chem. C 112 (2008) 5232–5240.
[33] M. Brown, S. Primdahl, M. Mogensen, J. Electrochem. Soc. 147 (2000) 475–485.
[34] R. Hui, Z. Wang, O. Kesler, L. Rose, J. Jankovic, S. Yick, R. Maric, D. Ghosh, J. Power Sources 170 (2007) 308–323.
[35] J.C. Ruiz-Morales, J.S. Canales-Vázquez, C. Savaniu, D. Marrero-López, W. Zhou, J.T.S. Irvine, Nature 439 (2006) 568–571.
[36] J. Liu, S.A. Barnett, Solid State Ionics 158 (2003) 11–16.
[37] T. Hibino, A. Hashimoto, K. Asano, M. Yano, M. Suzuki, M. Sano, Electrochem. Solid State Lett. 5 (2002) A242–A244.
[38] T. Hibino, A. Hashimoto, M. Yano, M. Suzuki, S.-I. Yoshida, M. Sano, J. Electrochem. Soc. 149 (2002) A133–A136.
[39] E.S. Putna, J. Stubenrauch, J.M. Vohs, R.J. Gorte, Langmuir 11 (1995) 4832–4837.